

Current Biology

The BORDER family of negative transcription elongation factors regulates flowering time in *Arabidopsis*

Highlights

- BDR proteins repress expression of the floral repressor, *FLC*
- BDR proteins physically interact with the autonomous pathway protein FPA
- BDR-repressed genes have high levels of Pol II occupancy, despite low mRNA levels
- Gene repression by BDR may involve the inhibition of transcription elongation

Authors

Xuhong Yu, Pascal G.P. Martin, Yixiang Zhang, ..., Yangnan Gu, Xingjun Wang, Scott D. Michaels

Correspondence

xuhongy@gmail.com (X.Y.),
michaels@indiana.edu (S.D.M.)

In brief

Yu et al. show that genes repressed by the BDR family of negative transcription elongation factors have high levels of Pol II occupancy, despite relatively low steady-state RNA levels. In this way, BDR proteins may allow for the later resumption of transcription or facilitate the long-term repression of genes by repressive histone modifications.



Report

The BORDER family of negative transcription elongation factors regulates flowering time in *Arabidopsis*

Xuhong Yu,^{1,10,*} Pascal G.P. Martin,^{1,8,10} Yixiang Zhang,² Jonathan C. Trinidad,^{2,3} Feifei Xu,⁴ Jie Huang,⁵ Karen E. Thum,^{1,9} Ke Li,¹ ShuZhen Zhao,⁶ Yangnan Gu,⁷ Xingjun Wang,⁶ and Scott D. Michaels^{1,11,*}

¹Department of Biology, Indiana University, 915 East Third Street, Bloomington, IN 47405, USA

²Department of Chemistry, Indiana University, Bloomington, IN 47405, USA

³Laboratory for Biological Mass Spectrometry, Department of Chemistry, Indiana University Bloomington, Bloomington, IN, USA

⁴Institute of Nuclear Agricultural Sciences, Key Laboratory for Nuclear Agricultural Sciences of Zhejiang Province and Ministry of Agriculture and Rural Affairs, Zhejiang University, Zijingang Campus, Hangzhou 310058, China

⁵Center for Genomics and Bioinformatics, Indiana University, 915 East Third Street, Bloomington, IN 47405, USA

⁶Shandong Provincial Key Laboratory of Crop Genetic Improvement, Ecology and Physiology, Biotechnology Research Center, Shandong Academy of Agricultural Sciences, Jinan 250100, China

⁷Department of Plant and Microbial Biology, University of California, Berkeley, Berkeley, CA 94720, USA

⁸Present address: INRAE, Université Bordeaux, UMR BFP, 33882 Villenave d'Ornon, France

⁹Present address: Stoller Enterprises, Houston, TX 77024, USA

¹⁰These authors contributed equally

¹¹Lead contact

*Correspondence: xuhongy@gmail.com (X.Y.), michaels@indiana.edu (S.D.M.)

<https://doi.org/10.1016/j.cub.2021.09.074>

SUMMARY

Transcription initiation has long been considered a primary regulatory step in gene expression. Recent work, however, shows that downstream events, such as transcription elongation, can also play important roles.^{1–3} A well-characterized example from animals is promoter-proximal pausing, where transcriptionally engaged Pol II accumulates 30–50 bp downstream of the transcription start site (TSS) and is thought to enable rapid gene activation.² Plants do not make widespread use of promoter-proximal pausing; however, in a phenomenon known as 3' pausing, a significant increase in Pol II is observed near the transcript end site (TES) of many genes.^{4–6} Previous work has shown that 3' pausing is promoted by the BORDER (BDR) family of negative transcription elongation factors. Here we show that BDR proteins play key roles in gene repression. Consistent with BDR proteins acting to slow or pause elongating Pol II, BDR-repressed genes are characterized by high levels of Pol II occupancy, yet low levels of mRNA. The BDR proteins physically interact with FPA,⁷ one of approximately two dozen genes collectively referred to as the autonomous floral-promotion pathway,⁸ which are necessary for the repression of the flowering time gene *FLOWERING LOCUS C (FLC)*.^{9–11} In early-flowering strains, *FLC* expression is repressed by repressive histone modifications, such as histone H3 lysine 27 trimethylation (H3K27me3), thereby allowing the plants to flower early. These results suggest that the repression of transcription elongation by BDR proteins may allow for the temporary pausing of transcription or facilitate the long-term repression of genes by repressive histone modifications.

RESULTS AND DISCUSSION

BDR proteins interact with autonomous pathway protein FPA

To investigate the molecular function of the autonomous pathway, we used yeast two-hybrid (Y2H) screens to identify binding partners of FPA.^{7,12} Two related proteins, BDR1 and BDR2, were identified as FPA interactors in the library screen. BDR1 and BDR2 belong to a three-member protein family that also includes BDR3.¹³ Although BDR3 was not identified in the screen, all three proteins can interact with FPA in Y2H assays (Figure 1A). BDR proteins each contain a SPOC domain, which is found in the SPEN family of transcriptional repressors, and a

TFIIS central domain (Figure 1C).^{14,15} Using truncated BDR proteins, we found that the amino terminal region and TFIIS central domain are dispensable for the interaction with FPA (Figures 1B and 1C). In contrast, deletions that removed the SPOC domain or its N-terminal extension failed to interact. For BDR2, we also identified an alternatively spliced form (BDR2as) with a frameshift that removes the SPOC and C-terminal domains (Figure 1C). This form did not interact with FPA (Figure 1A).

For BDR3, we found a one-base deletion relative to the reference TAIR10 assembly, creating a frameshift that extends the open reading frame by 145 amino acids, a sequence displaying homology to the C-terminal regions of BDR1 and BDR2. In Y2H assays, full-length BDR3 interacted with FPA, but a truncated



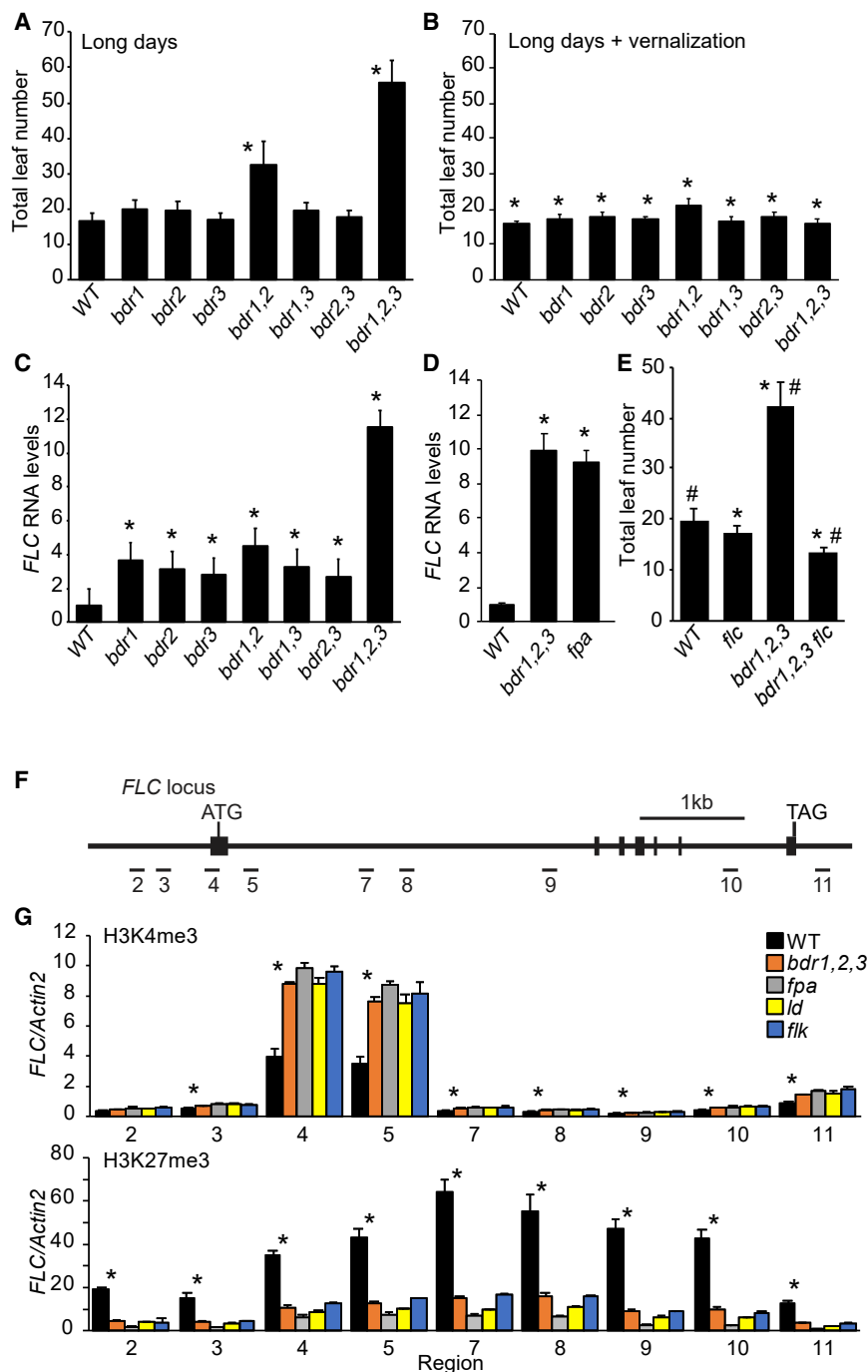


Figure 2. *bdr* mutants are late flowering and fail to repress *FLC*

(A) Flowering time of single and higher-order *BDR* mutants. (B) The late-flowering phenotype of *bdr* mutants is eliminated by vernalization. (C) *bdr* mutations result in elevated *FLC* levels, as determined by qRT-PCR. (D) *FLC* levels in the *bdr1,2,3* triple mutant are similar to that found in *fpa*. (E) The late-flowering phenotype of *bdr1,2,3* is *FLC*-dependent. (F) Schematic drawing of the *FLC* locus. The locations of primers used for qPCR are numbered. (G) ChIP-qPCR analysis of the *FLC* locus using antibodies recognizing H3K4me3 or H3K27me3. Error bars indicate one standard deviation. Asterisks indicate a significant difference from wild type (A and C–E) or non-vernalized samples (B). # indicates a significant difference from *flc-3* (G). Asterisks indicate a significant difference between wild type and *bdr1,2,3*. Student's *t* test, *p* < 0.01. See also Figure S1.

and the autonomous-pathway mutants *fpa*, *ld*, and *flk* showed similar patterns of reduced levels of H3K27me3 and increased H3K4me3 (Figures 2F and 2G). Thus, like other members of the autonomous pathway, BDR proteins are required for the deposition of repressive histone modifications at *FLC*.

BDR proteins and FPA show overlapping chromatin localization and effects on transcription

To determine if BDR proteins and FPA have overlapping binding sites, we performed ChIP sequencing (ChIP-seq) using an antibody recognizing FPA. Consistent with its proposed role in 3' end processing,^{17,18} FPA occupancy was highest just downstream of the transcription end site (TES) (Figure 3A). Similar to BDR proteins,¹³ FPA binding was proportional to steady-state mRNA levels. To examine the correlation between FPA and BDR localization, we sorted genes by FPA level and generated heatmaps of BDR occupancy. At the 3'

body of *FLC* and gene expression is low. In autonomous-pathway mutants, H3K27me3 is strongly reduced and the activating H3K4me3 is enriched near the transcription start site (TSS), leading to increased *FLC* expression. To determine if the BDR proteins play a similar role in the repression of *FLC*, we examined the levels of H3K4me3 and H3K27me3 by chromatin immunoprecipitation (ChIP) followed by qPCR. Consistent with previous studies,¹¹ wild-type plants were enriched in H3K27me3 across the *FLC* locus and showed low H3K4me3 in the 5' region (Figures 2F and 2G). The *bdr1,2,3* triple mutant

ends of genes, there was a strong correlation of FPA and BDR protein occupancy (Figure 3C). Metaprofiles also showed peaks of FPA ChIP-seq signal at peaks of BDR1, BDR2, or BDR3 and vice versa (Figures S2A and S2B). Consistent with the correlation between FPA binding and mRNA levels, FPA occupancy was also correlated with RNA polymerase II (Pol II) occupancy (Figure 3C). Although FPA shows overlapping binding with the BDR proteins, FPA occupancy was largely unaffected in the *bdr1,2,3* mutant (Figure S2C). Thus, the BDR proteins are not required for the recruitment of FPA to chromatin. Overall, FPA

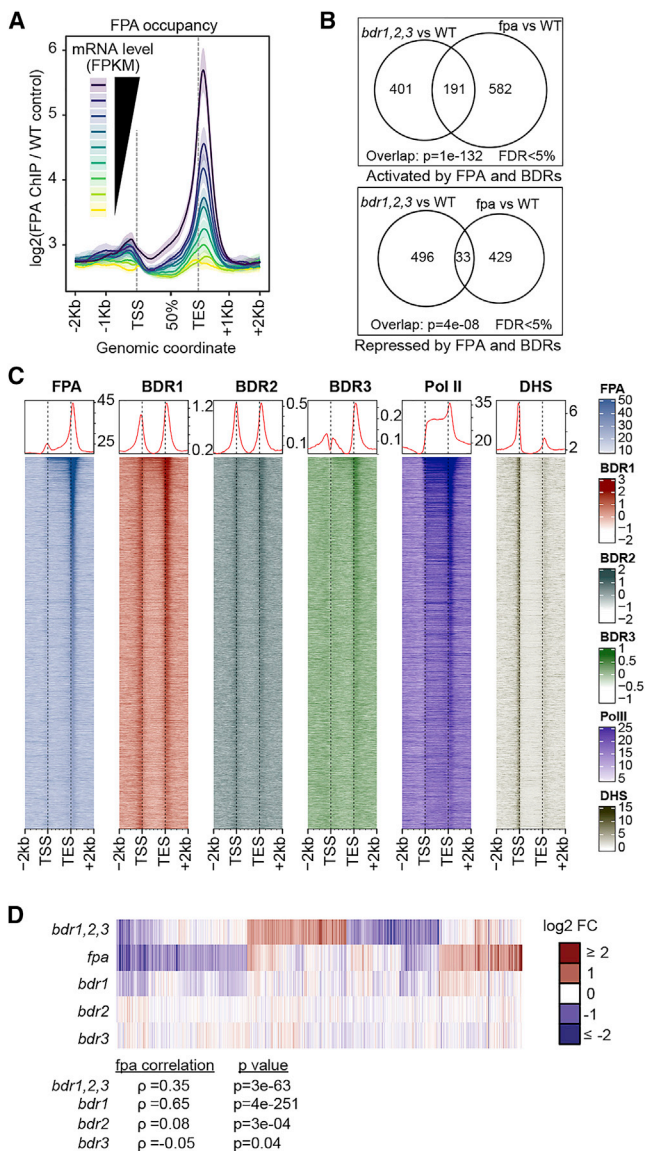


Figure 3. BDR proteins and FPA have overlapping localization and effects on expression

(A) Metagenes profiles of FPA ChIP-seq signal in nine groups of genes defined by increasing mRNA expression levels in wild type (FPKM, fragments per kilobase per million aligned fragments). Average signal (line) and associated 95% confidence interval based on a Gaussian assumption (shade) are represented. Signal in gene bodies was averaged in bins of 1% of the gene size. (B) Venn diagram showing the overlap between genes activated or repressed by BDR proteins and FPA.

(C) Heatmap and metagenes profiles (top) of ChIP-seq signals and DNase-hypersensitive sites (DHS). Genes were sorted by total FPA signal; the top 10,000 genes are shown.

(D) Identification of BDR and FPA-regulated genes by RNA-seq analysis. Genes significantly regulated in at least one genotype are shown (FDR < 5%). The Spearman rank correlation coefficient and its significance evaluate the similarity of gene expression changes occurring in *bdr* mutants compared to *fpa* mutant.

See also Figure S2 and Table S2.

and BDR proteins show overlapping patterns of chromatin localization; however, FPA has a strong preference for TESs, whereas BDR1 and BDR2 are enriched at both TSS and TES regions.¹³

We also found evidence for overlapping effects of BDR proteins and FPA on gene expression via RNA-seq. There was a significant overlap in genes with decreased or increased mRNA levels in *bdr1,2,3* or *fpa* (Figure 3B; Table S2). The overlap was greatest, however, for activated genes. Among *bdr* single mutants, the *fpa* mutant was most similar to *bdr1* in terms of changes in mRNA levels (Figure 3D). We were unable to recover an *fpa bdr1,2,3* quadruple mutant, possibly due to lethality. Unlike BDR-activated genes, which preferentially have an upstream neighbor transcribed from the same strand,¹³ FPA-activated genes did not show a strong bias for the orientation of the upstream gene (Figure S2D). FPA-activated genes did, however, show a slight preference for having a downstream neighbor on the opposite strand (Figure S2D), suggesting that FPA may be important in regions containing converging TESs. This would be consistent with recent work showing that other autonomous pathway proteins, such as LD and FLD, play roles in the regulation of convergent genes.¹⁹

BDR-repressed genes are characterized by high levels of Pol II occupancy but low steady-state mRNA levels

Given that BDR proteins prevent transcriptional interference by repressing Pol II elongation,¹³ we wondered if the repression of Pol II elongation might also help to explain the behavior of BDR-repressed genes. We determined Pol II occupancy by ChIP-seq in wild-type plants using antibodies recognizing Pol II, serine 5-phosphorylated Pol II (enriched in initiation), or serine 2-phosphorylated Pol II (associated with elongation).²⁰ As expected, Pol II occupancy correlates well with mRNA levels (Figure 4A). The 5% of genes with the highest mRNA levels showed approximately four times higher Pol II signal than the average of all genes. As expected, non-expressed genes showed little Pol II binding.

We then examined Pol II occupancy at BDR-repressed genes. Compared to BDR-activated genes or non-differentially expressed (non-DE) control genes, BDR repressed genes had much higher Pol II occupancy in wild type (Figure 4A), nearly as high as the top 5% of genes with the highest mRNA levels. This result was unexpected as the mRNA levels of the top 5% are ~75-fold higher than the mRNA levels of BDR-repressed genes (Figure 4B). BDR-repressed genes also had significantly lower mRNA levels than BDR-activated genes ($p = 3e-41$, Mann-Whitney test) or non-DE control genes ($p = 2e-26$), despite having higher levels of Pol II on their gene bodies (Figures 4A and 4B). We also noted differences in the distribution of Pol II across the groups of genes. For the top 5% most highly expressed genes, the average of all genes, and non-DE controls, Pol II was relatively evenly distributed across gene bodies with a peak just after the annotated TES (Figure 4A, red arrow). BDR-repressed genes, in contrast, had lower Pol II occupancy in the 3' portion of the gene, including the peak associated with 3' pausing. To further investigate the role of BDR proteins in transcription elongation, we examined BDR-repressed genes in published 5' GRO-seq and GRO-seq datasets.⁵ Little difference was observed between BDR-repressed genes and controls in 5' GRO-seq, suggesting comparable rates of initiation (Figures

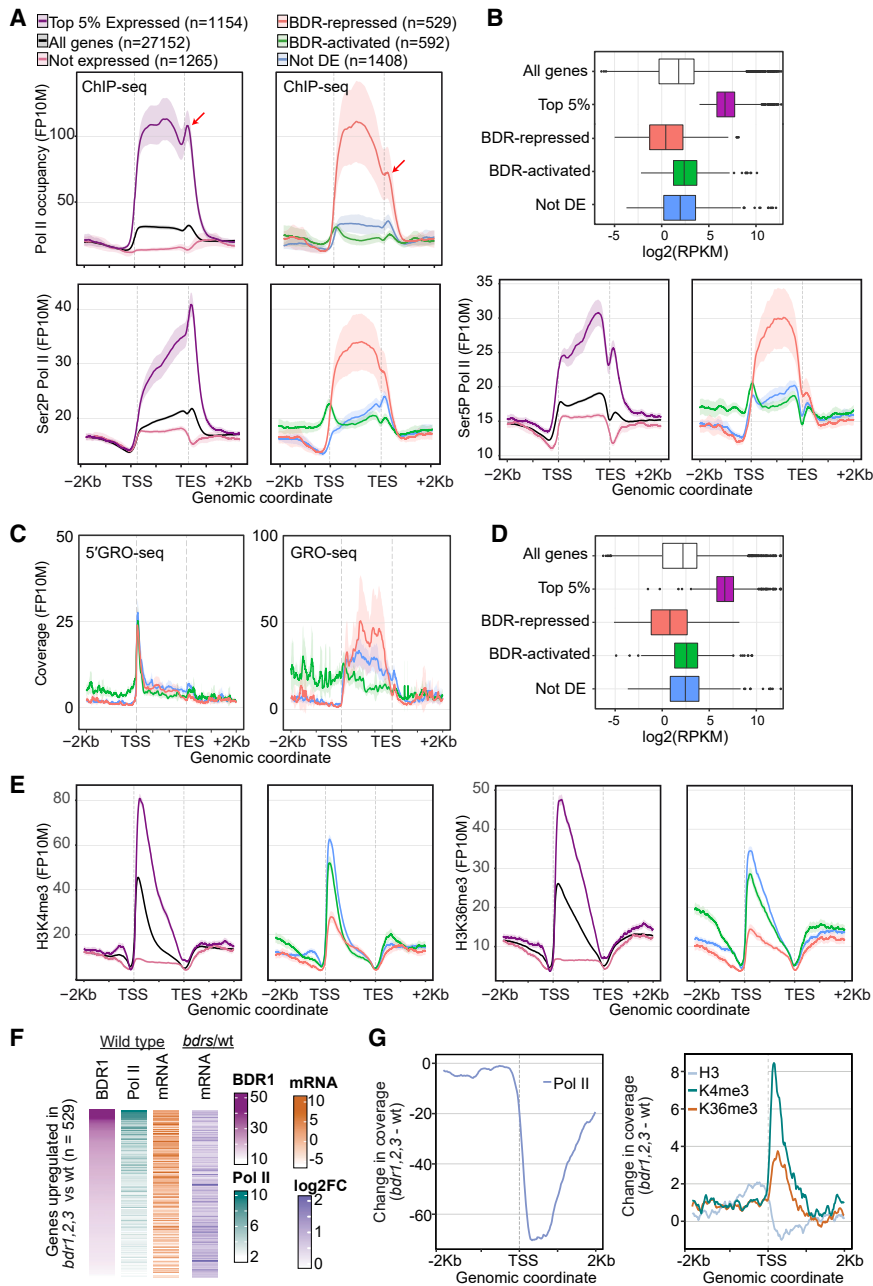


Figure 4. BDR-repressed genes have high Pol II occupancy, yet low levels of expression and signatures of repressed chromatin (A and C) Metagenome profiles of Pol II ChIP-seq (A), 5' GRO-seq, or GRO-seq coverage (C) across the indicated groups of genes in *Arabidopsis* seedlings. Red arrows indicate 3' pausing. (B and D) Boxplots showing the mRNA levels for Pol II ChIP-seq (B) or 5' GRO-seq/GRO-seq (D) samples for the indicated gene classes. Differences are evaluated by Wilcoxon rank-sum test. (E) Metagenome profiles of histone modifications across the groups of genes indicated in (A). (F) BDR-repressed genes were sorted by BDR1 occupancy. Levels of BDR1, Pol II, and mRNA levels are shown for wild type. Also shown is the change in mRNA levels for BDR-repressed genes (*bdr1,2,3/wt*). (G) Plots showing the change in Pol II occupancy (*bdr1,2,3/wt*) and histone modifications around the TSS of BDR-repressed genes. See also Figure S3.

states are achieved is still an active area of research, but the process appears to be dependent on the recruitment of histone-modifying enzymes, transcription turn over, and Pol II transcription rate.^{22,23} Given the high levels of Pol II, yet low levels of mRNA, observed from BDR-repressed genes, we wondered whether histone modifications at these genes would resemble those of actively expressed genes or repressed genes.

We used ChIP-seq to determine levels of histone modifications in wild-type plants (Figures 4E and S3A). A clear correlation was observed between mRNA levels and H3K4me3 and H3K36me3 for non-expressed genes, the average of all genes, and the genes in the top 5% for mRNA level (Figure 4E). Despite having higher Pol II occupancy than BDR-protected or non-DE genes (Figure 4A), BDR-repressed genes had much lower levels of H3K4me3 and H3K36me3 (Figure 4E). Thus, the chromatin state of

BDR-repressed genes is better correlated with their relatively low mRNA levels than with their high Pol II occupancy. Given the model that both the recruitment of Pol II-associated chromatin modifiers and repeated rounds of transcription are required for the effective deposition of histone modifications,²³ our data suggest that transcription turnover may be the limiting factor in the deposition of H3K4me3 and H3K36me3 at BDR-repressed genes.

Histone modifications at BDR-repressed genes are more reflective of gene expression levels than Pol II levels

It is well established that specific post-translational histone modifications, such as H3K4 or H3K36 methylation, are deposited during transcription elongation via the physical interaction of Pol II with “epigenetic writers.”²¹ The details of how these chromatin

BDR-repressed genes is better correlated with their relatively low mRNA levels than with their high Pol II occupancy. Given the model that both the recruitment of Pol II-associated chromatin modifiers and repeated rounds of transcription are required for the effective deposition of histone modifications,²³ our data suggest that transcription turnover may be the limiting factor in the deposition of H3K4me3 and H3K36me3 at BDR-repressed genes.

In the *bdr* mutant, Pol II decreases at BDR-repressed genes while mRNA levels increase

Taken together, the results above suggest that BDR proteins repress gene expression by impeding Pol II elongation, which

leads to high Pol II occupancy at BDR-repressed genes. If this model is correct, more efficient transcription of BDR-repressed genes in the *bdr1,2,3* mutant may lead to higher mRNA levels, yet lower levels of Pol II occupancy. To test this hypothesis, we compared Pol II occupancy in wild type and *bdr1,2,3*. We sorted BDR-repressed genes, all of which show increased mRNA levels in the *bdr1,2,3* mutant, by BDR1 occupancy (Figure 4F). In wild type, a positive correlation was observed between BDR1 occupancy and Pol II occupancy, particularly for genes with the highest levels of BDR1 (Figures 4F and S3B). There was not a strong correlation between BDR1 and Pol II occupancy and mRNA level in wild type (Figure 4F) nor with the amplitude of change in mRNA level between *bdr1,2,3* and wild type. Consistent with our model, Pol II occupancy dropped at BDR-repressed genes in the *bdr1,2,3* mutant (Figures 4G and S3C). The decrease in Pol II was most pronounced in genes with the highest BDR1 occupancy, which are the most likely direct targets of BDR1. H3K4me3 and H3K36me3 also increased at these genes in the *bdr1,2,3* mutant, suggesting that increased transcription turnover may be important in establishing these modifications at BDR-repressed genes (Figures 4G and S3C). Overall, these data indicate that BDR proteins impede the efficient elongation by Pol II, leading to lower transcript accumulation and reduced accumulation of activating histone modifications.

In conclusion, this work supports a model in which BDR proteins repress gene expression by acting as negative transcription elongation factors. There are similarities and differences between promoter-proximal pausing in animals and the repression of gene expression by BDR proteins. Both mechanisms feature high Pol II occupancy within genes with low mRNA levels, but with different distributions along gene bodies. Promoter-proximal pausing involves NELF, which is absent in plants, and results in the accumulation of engaged Pol II at a discrete pausing site near the promoter.²⁴ BDR proteins, in contrast, promote a broad accumulation of paused or slow Pol II across the body of BDR-repressed genes. In animals, the release of promoter-proximal pausing by P-TEFb is thought to provide a means of rapid and coordinated gene activation (e.g., heat shock genes in *Drosophila*).²⁵ Additional investigation will be required to determine if BDR-mediated Pol II pausing might also serve as a means for the rapid activation of gene expression.

In addition to potentially allowing for future resumption of transcription, the repression of transcription elongation by BDR proteins could also facilitate the long-term repression of genes by repressive histone modifications. The deposition of H3K27me3 by PRC2 is inhibited by pre-existing H3K4me3.²⁶ When genes are actively expressed, the repeated passage of Pol II and associated chromatin modifiers serves to reinforce the deposition of H3K4me3. By inhibiting the progression of Pol II, BDR proteins may provide an opportunity for the removal of H3K4me3, thus providing a suitable substrate for PRC2. This may be the case for the repression of *FLC* by BDR proteins and the autonomous pathway. Both mathematical modeling and experimental investigations have shown that *FLC* regulation by the autonomous pathway is linked to coordinated changes in initiation, elongation rate, termination, antisense transcription, and chromatin modifications and architecture.^{18,27–29} Although the precise order of

events is still being elucidated, the repression of Pol II elongation by the BDR proteins may coordinate some of these molecular events at the *FLC* locus. For example, by inhibiting transcription cycles at *FLC*, BDR proteins could facilitate the removal of H3K4 methylation by the autonomous pathway histone demethylase FLD, enabling silencing by H3K27me3.

STAR★METHODS

Detailed methods are provided in the online version of this paper and include the following:

- KEY RESOURCES TABLE
- RESOURCE AVAILABILITY
 - Lead contact
 - Materials Availability
 - Data and code availability
- EXPERIMENTAL MODEL AND SUBJECT DETAILS
- METHOD DETAILS
 - Plant growth conditions
 - Constructs
 - Y2H
 - BiFC
 - Co-immunoprecipitation and mass spectrometry
 - RNA expression analysis
 - RNA-seq
 - ChIP-qPCR
 - ChIP-seq
 - Reanalysis of published datasets
 - Bioinformatic analyses
- QUANTIFICATION AND STATISTICAL ANALYSIS

SUPPLEMENTAL INFORMATION

Supplemental information can be found online at <https://doi.org/10.1016/j.cub.2021.09.074>.

ACKNOWLEDGMENTS

Next-generation sequencing was performed at the Indiana University Center for Genomics and Bioinformatics. We thank Stephanie M. DeYoung and Laurel B. Bender for assistance with Y2H screening and antibody generation. We are grateful to the GenoToul bioinformatics platform Toulouse Midi-Pyrenees (Bioinfo GenoToul) for providing computing and storage resources. This work was supported by grants to S.D.M. from the National Institutes of Health (GM075060), National Science Foundation (2001115), and the Indiana Clinical and Translational Sciences Institute and to Y.G. from the USDA National Institute of Food and Agriculture (CA-B-PLB-0243-H) and the National Science Foundation (2049931). P.G.P.M. received the support of the EU in the framework of the Marie-Curie FP7 COFUND People Programme, through the award of an AgreeSkills+ fellowship (under grant agreement no. 609398).

AUTHOR CONTRIBUTIONS

X.Y., P.G.P.M., Y.G., X.W., F.X., and S.D.M. participated in the design of experiments. Y.Z. and J.C.T. performed mass spectrometry. X.Y., J.H., and P.G.P.M. created sequencing libraries and P.G.P.M. performed bioinformatic analyses. K.E.T., K.L., and S.Z. performed experiments. X.Y., P.G.P.M., and S.D.M. were responsible for writing and overall direction of the project.

DECLARATION OF INTERESTS

The authors declare no competing interests.

Received: February 8, 2021
Revised: July 20, 2021
Accepted: September 27, 2021
Published: October 18, 2021

REFERENCES

- Adelman, K., and Lis, J.T. (2012). Promoter-proximal pausing of RNA polymerase II: emerging roles in metazoans. *Nat. Rev. Genet.* *13*, 720–731.
- Gaertner, B., and Zeitlinger, J. (2014). RNA polymerase II pausing during development. *Development* *141*, 1179–1183.
- Gilchrist, D.A., and Adelman, K. (2012). Coupling polymerase pausing and chromatin landscapes for precise regulation of transcription. *Biochim. Biophys. Acta* *1819*, 700–706.
- Zhu, J., Liu, M., Liu, X., and Dong, Z. (2018). RNA polymerase II activity revealed by GRO-seq and pNET-seq in Arabidopsis. *Nat. Plants* *4*, 1112–1123.
- Hetzl, J., Duttke, S.H., Benner, C., and Chory, J. (2016). Nascent RNA sequencing reveals distinct features in plant transcription. *Proc. Natl. Acad. Sci. USA* *113*, 12316–12321.
- Erhard, K.F., Jr., Talbot, J.E., Deans, N.C., McClish, A.E., and Hollick, J.B. (2015). Nascent transcription affected by RNA polymerase IV in *Zea mays*. *Genetics* *199*, 1107–1125.
- Schomburg, F.M., Patton, D.A., Meinke, D.W., and Amasino, R.M. (2001). FPA, a gene involved in floral induction in Arabidopsis, encodes a protein containing RNA-recognition motifs. *Plant Cell* *13*, 1427–1436.
- Wu, Z., Fang, X., Zhu, D., and Dean, C. (2020). Autonomous pathway: FLOWERING LOCUS C repression through an antisense-mediated chromatin-silencing mechanism. *Plant Physiol.* *182*, 27–37.
- Michaels, S.D., and Amasino, R.M. (1999). FLOWERING LOCUS C encodes a novel MADS domain protein that acts as a repressor of flowering. *Plant Cell* *11*, 949–956.
- Sheldon, C.C., Burn, J.E., Perez, P.P., Metzger, J., Edwards, J.A., Peacock, W.J., and Dennis, E.S. (1999). The FLF MADS box gene: a repressor of flowering in Arabidopsis regulated by vernalization and methylation. *Plant Cell* *11*, 445–458.
- Whittaker, C., and Dean, C. (2017). The FLC locus: a platform for discoveries in epigenetics and adaptation. *Annu. Rev. Cell Dev. Biol.* *33*, 555–575.
- Meier, C., Bouquin, T., Nielsen, M.E., Raventos, D., Mattsson, O., Rocher, A., Schomburg, F., Amasino, R.M., and Mundy, J. (2001). Gibberellin response mutants identified by luciferase imaging. *Plant J.* *25*, 509–519.
- Yu, X., Martin, P.G.P., and Michaels, S.D. (2019). BORDER proteins protect expression of neighboring genes by promoting 3' Pol II pausing in plants. *Nat. Commun.* *10*, 4359.
- Chédin, S., Riva, M., Schultz, P., Sentenac, A., and Carles, C. (1998). The RNA cleavage activity of RNA polymerase III is mediated by an essential TFIIIS-like subunit and is important for transcription termination. *Genes Dev.* *12*, 3857–3871.
- Ariyoshi, M., and Schwabe, J.W. (2003). A conserved structural motif reveals the essential transcriptional repression function of Spen proteins and their role in developmental signaling. *Genes Dev.* *17*, 1909–1920.
- Michaels, S.D., and Amasino, R.M. (2001). Loss of FLOWERING LOCUS C activity eliminates the late-flowering phenotype of FRIGIDA and autonomous pathway mutations but not responsiveness to vernalization. *Plant Cell* *13*, 935–941.
- Duc, C., Sherstnev, A., Cole, C., Barton, G.J., and Simpson, G.G. (2013). Transcription termination and chimeric RNA formation controlled by Arabidopsis thaliana FPA. *PLoS Genet.* *9*, e1003867.
- Sonmez, C., Bäurle, I., Magusin, A., Dreos, R., Laubinger, S., Weigel, D., and Dean, C. (2011). RNA 3' processing functions of Arabidopsis FCA and FPA limit intergenic transcription. *Proc. Natl. Acad. Sci. USA* *108*, 8508–8513.
- Inagaki, S., Takahashi, M., Takashima, K., Oya, S., and Kakutani, T. (2021). Chromatin-based mechanisms to coordinate convergent overlapping transcription. *Nat. Plants* *7*, 295–302.
- Phatnani, H.P., and Greenleaf, A.L. (2006). Phosphorylation and functions of the RNA polymerase II CTD. *Genes Dev.* *20*, 2922–2936.
- Smolle, M., and Workman, J.L. (2013). Transcription-associated histone modifications and cryptic transcription. *Biochim. Biophys. Acta* *1829*, 84–97.
- Fong, N., Saldi, T., Sheridan, R.M., Cortazar, M.A., and Bentley, D.L. (2017). RNA Pol II dynamics modulate co-transcriptional chromatin modification, CTD phosphorylation, and transcriptional direction. *Mol. Cell* *66*, 546–557.e3.
- Soares, L.M., He, P.C., Chun, Y., Suh, H., Kim, T., and Buratowski, S. (2017). Determinants of histone H3K4 methylation patterns. *Mol. Cell* *68*, 773–785.e6.
- Levine, M. (2011). Paused RNA polymerase II as a developmental checkpoint. *Cell* *145*, 502–511.
- Fuda, N.J., Ardehali, M.B., and Lis, J.T. (2009). Defining mechanisms that regulate RNA polymerase II transcription in vivo. *Nature* *461*, 186–192.
- Schmitges, F.W., Prusty, A.B., Faty, M., Stützer, A., Lingaraju, G.M., Aiwazian, J., Sack, R., Hess, D., Li, L., Zhou, S., et al. (2011). Histone methylation by PRC2 is inhibited by active chromatin marks. *Mol. Cell* *42*, 330–341.
- Fang, X., Wu, Z., Raitskin, O., Webb, K., Voigt, P., Lu, T., Howard, M., and Dean, C. (2020). The 3' processing of antisense RNAs physically links to chromatin-based transcriptional control. *Proc. Natl. Acad. Sci. USA* *117*, 15316–15321.
- Jégu, T., Latrasse, D., Delarue, M., Hirt, H., Domenichini, S., Ariel, F., Crespi, M., Bergounioux, C., Raynaud, C., and Benhamed, M. (2014). The BAF60 subunit of the SWI/SNF chromatin-remodeling complex directly controls the formation of a gene loop at FLOWERING LOCUS C in Arabidopsis. *Plant Cell* *26*, 538–551.
- Wu, Z., Ietswaart, R., Liu, F., Yang, H., Howard, M., and Dean, C. (2016). Quantitative regulation of FLC via coordinated transcriptional initiation and elongation. *Proc. Natl. Acad. Sci. USA* *113*, 218–223.
- Van Larebeke, N., Engler, G., Holsters, M., Van den Elsacker, S., Zaenen, I., Schilperoort, R.A., and Schell, J. (1974). Large plasmid in *Agrobacterium tumefaciens* essential for crown gall-inducing ability. *Nature* *252*, 169–170.
- Yu, X., and Michaels, S.D. (2010). The Arabidopsis Paf1c complex component CDC73 participates in the modification of FLOWERING LOCUS C chromatin. *Plant Physiol.* *153*, 1074–1084.
- Gampala, S.S., Kim, T.W., He, J.X., Tang, W., Deng, Z., Bai, M.Y., Guan, S., Lalonde, S., Sun, Y., Gendron, J.M., et al. (2007). An essential role for 14-3-3 proteins in brassinosteroid signal transduction in Arabidopsis. *Dev. Cell* *13*, 177–189.
- Xie, Q., Frugis, G., Colgan, D., and Chua, N.H. (2000). Arabidopsis NAC1 transduces auxin signal downstream of TIR1 to promote lateral root development. *Genes Dev.* *14*, 3024–3036.
- Dobin, A., Davis, C.A., Schlesinger, F., Drenkow, J., Zaleski, C., Jha, S., Batut, P., Chaisson, M., and Gingeras, T.R. (2013). STAR: ultrafast universal RNA-seq aligner. *Bioinformatics* *29*, 15–21.
- Li, H., Handsaker, B., Wysoker, A., Fennell, T., Ruan, J., Homer, N., Marth, G., Abecasis, G., and Durbin, R.; 1000 Genome Project Data Processing Subgroup (2009). The Sequence Alignment/Map format and SAMtools. *Bioinformatics* *25*, 2078–2079.
- Liao, Y., Smyth, G.K., and Shi, W. (2014). featureCounts: an efficient general purpose program for assigning sequence reads to genomic features. *Bioinformatics* *30*, 923–930.
- Liao, Y., Smyth, G.K., and Shi, W. (2019). The R package Rsubread is easier, faster, cheaper and better for alignment and quantification of RNA sequencing reads. *Nucleic Acids Res.* *47*, e47.
- Lawrence, M., Huber, W., Pagès, H., Aboyoun, P., Carlson, M., Gentleman, R., Morgan, M.T., and Carey, V.J. (2013). Software for

- computing and annotating genomic ranges. *PLoS Comput. Biol.* 9, e1003118.
39. Love, M.I., Huber, W., and Anders, S. (2014). Moderated estimation of fold change and dispersion for RNA-seq data with DESeq2. *Genome Biol.* 15, 550.
 40. Bolger, A.M., Lohse, M., and Usadel, B. (2014). Trimmomatic: a flexible trimmer for Illumina sequence data. *Bioinformatics* 30, 2114–2120.
 41. Langmead, B., and Salzberg, S.L. (2012). Fast gapped-read alignment with Bowtie 2. *Nat. Methods* 9, 357–359.
 42. Lawrence, M., Gentleman, R., and Carey, V. (2009). rtracklayer: an R package for interfacing with genome browsers. *Bioinformatics* 25, 1841–1842.
 43. Gu, Z., Eils, R., Schlesner, M., and Ishaque, N. (2018). EnrichedHeatmap: an R/Bioconductor package for comprehensive visualization of genomic signal associations. *BMC Genomics* 19, 234.
 44. Cho, Y.H., Yoo, S.D., and Sheen, J. (2006). Regulatory functions of nuclear hexokinase1 complex in glucose signaling. *Cell* 127, 579–589.
 45. Ream, T.S., Haag, J.R., Wierzbicki, A.T., Nicora, C.D., Norbeck, A.D., Zhu, J.K., Hagen, G., Guilfoyle, T.J., Pasa-Tolić, L., and Pikaard, C.S. (2009). Subunit compositions of the RNA-silencing enzymes Pol IV and Pol V reveal their origins as specialized forms of RNA polymerase II. *Mol. Cell* 33, 192–203.
 46. Feys, B.J., Moisan, L.J., Newman, M.A., and Parker, J.E. (2001). Direct interaction between the Arabidopsis disease resistance signaling proteins, EDS1 and PAD4. *EMBO J.* 20, 5400–5411.
 47. Zemach, A., Kim, M.Y., Hsieh, P.H., Coleman-Derr, D., Eshed-Williams, L., Thao, K., Harmer, S.L., and Zilberman, D. (2013). The Arabidopsis nucleosome remodeler DDM1 allows DNA methyltransferases to access H1-containing heterochromatin. *Cell* 153, 193–205.
 48. Bernatavichute, Y.V., Zhang, X., Cokus, S., Pellegrini, M., and Jacobsen, S.E. (2008). Genome-wide association of histone H3 lysine nine methylation with CHG DNA methylation in Arabidopsis thaliana. *PLoS ONE* 3, e3156.
 49. Parker, M.T., Knop, K., Zacharaki, V., Sherwood, A.V., Tomé, D., Yu, X., Martin, P.G., Beynon, J., Michaels, S.D., Barton, G.J., and Simpson, G.G. (2021). Widespread premature transcription termination of *Arabidopsis thaliana* NLR genes by the spen protein FPA. *eLife* 10, e65537.
 50. Zhang, W., Zhang, T., Wu, Y., and Jiang, J. (2012). Genome-wide identification of regulatory DNA elements and protein-binding footprints using signatures of open chromatin in Arabidopsis. *Plant Cell* 24, 2719–2731.
 51. Langmead, B., Trapnell, C., Pop, M., and Salzberg, S.L. (2009). Ultrafast and memory-efficient alignment of short DNA sequences to the human genome. *Genome Biol.* 10, R25.
 52. Huber, W., Carey, V.J., Gentleman, R., Anders, S., Carlson, M., Carvalho, B.S., Bravo, H.C., Davis, S., Gatto, L., Girke, T., et al. (2015). Orchestrating high-throughput genomic analysis with Bioconductor. *Nat. Methods* 12, 115–121.
 53. Zhang, Y., Liu, T., Meyer, C.A., Eickhoute, J., Johnson, D.S., Bernstein, B.E., Nusbaum, C., Myers, R.M., Brown, M., Li, W., and Liu, X.S. (2008). Model-based analysis of ChIP-seq (MACS). *Genome Biol.* 9, R137.

STAR★METHODS

KEY RESOURCES TABLE

| REAGENT or RESOURCE | SOURCE | IDENTIFIER |
|---|---------------------|--------------------------------|
| Antibodies | | |
| anti-HA-peroxidase | Sigma | Cat# H6533; RRID: AB_439705 |
| anti-c-Myc-peroxidase | Sigma | Cat# 16-213; RRID :AB_310809 |
| anti-FPA | This study | N/A |
| anti-Histone H3 | Abcam | Cat# ab1791; RRID: AB_302613 |
| anti-Histone H3 (tri methyl K36) | Abcam | Cat# ab9050; RRID: AB_306966 |
| anti-Histone H3 (tri methyl K4) | Millipore | Cat# 17-614; RRID: AB_11212770 |
| anti-Histone H3 (di methyl K4) | Millipore | Cat# 17-677; RRID: AB_1977530 |
| anti-Histone H3 (tri methyl K27) | Millipore | Cat# 07-449; RRID: AB_310624 |
| Bacterial and virus strains | | |
| <i>Agrobacterium tumefaciens</i> C58C1 | ³⁰ | N/A |
| <i>Escherichia coli</i> TOP10 | Invitrogen | C404010 |
| Chemicals, peptides, and recombinant proteins | | |
| Plant Protease Inhibitors | Sigma | P9599 |
| SuperSignal West Pico Chemiluminescent Substrate | Thermo | PI34580 |
| Murashige and Skoog medium | VWR | IC2610024 |
| Protein A agarose | Thermo | 15918-014 |
| Critical commercial assays | | |
| NEBNext Ultra DNA Library Prep kit | New England Biolabs | E7645S |
| Platinum SYBR Green qPCR SuperMix-UDG kit | Thermo | 11733038 |
| Deposited data | | |
| Gene expression profiling in wild-type, <i>fpa</i> mutant and <i>bdrs</i> triple mutant <i>Arabidopsis</i> seedlings | ¹³ | GEO: GSE112440 |
| Gene expression profiling by RNA-seq of wild-type, <i>fpa</i> mutant, <i>bdr1</i> mutant, <i>bdr2</i> mutant, <i>bdr3</i> mutant and <i>bdrs</i> triple mutant <i>Arabidopsis</i> seedlings | ¹³ | GEO: GSE112441 |
| Genome-wide profiling of nucleosomes (MNase-seq), total H3, H3K4me2, H3K4me3 and H3K36me3 (native ChIP-seq) in wild-type, <i>fpa</i> mutant and <i>bdrs</i> triple mutant | ¹³ | GEO: GSE113076 |
| Genome-wide occupancy of BDR1, BDR2 and FPA (ChIP-seq) | ¹³ | GEO: GSE113059 |
| Genome-wide profiling (ChIP-seq) of RNA polymerase II in wild-type, <i>fpa</i> mutant and <i>bdrs</i> triple mutant | ¹³ | GEO: GSE113078 |
| Genome-wide occupancy of BDR1 and BDR3 (ChIP-seq) | ¹³ | GEO: GSE131772 |
| Experimental models: Organisms/strains | | |
| <i>Arabidopsis thaliana</i> : Col-0 | Widely distributed | N/A |
| <i>Nicotiana benthamiana</i> | Widely distributed | N/A |
| <i>Arabidopsis</i> : <i>fpa-7</i> | ³¹ | N/A |
| <i>Arabidopsis</i> : <i>flk</i> | ³¹ | N/A |
| <i>Arabidopsis</i> : <i>ld-1</i> | ³¹ | N/A |
| <i>Arabidopsis</i> : <i>flc-3</i> | ³¹ | N/A |
| <i>Arabidopsis</i> : <i>bdr1-1</i> | ¹³ | N/A |
| <i>Arabidopsis</i> : <i>bdr2-1</i> | ¹³ | N/A |
| <i>Arabidopsis</i> : <i>bdr3-1</i> | ¹³ | N/A |
| <i>Arabidopsis</i> : <i>bdr1,2,3</i> | ¹³ | N/A |

(Continued on next page)

Continued

| REAGENT or RESOURCE | SOURCE | IDENTIFIER |
|---|-----------------|---|
| Oligonucleotides | | |
| See Table S3 | This study | N/A |
| Recombinant DNA | | |
| pENTR/D-TOPO | Invitrogen | K2400-20 |
| pDEST22 | Invitrogen | PQ1000101 |
| pDEST32 | Invitrogen | PQ1000101 |
| pNYFP-X-gw | 32 | N/A |
| pCCFP-X-gw | 32 | N/A |
| BDR1-MYC | 13 | N/A |
| BDR2-MYC | 13 | N/A |
| BDR3-MYC | 13 | N/A |
| pDEST32-FPA | This study | N/A |
| pDEST22-BDR1 | This study | N/A |
| pDEST22-BDR2 | This study | N/A |
| pDEST22-BDR3 | This study | N/A |
| pDEST22-BDR2as | This study | N/A |
| pDEST22-BDR3t | This study | N/A |
| pDEST22-BDR1 N517 | This study | N/A |
| pDEST22-BDR1 N650 | This study | N/A |
| pDEST22-BDR1 N760 | This study | N/A |
| pDEST22-BDR2 N381 | This study | N/A |
| pDEST22-BDR2 N413 | This study | N/A |
| pDEST22-BDR2 N483 | This study | N/A |
| pDEST22-BDR2 N540 | This study | N/A |
| pDEST22-BDR2 N650 | This study | N/A |
| pNYFP-FPA | This study | N/A |
| pCCFP-BDR1 | This study | N/A |
| pCCFP-BDR2 | This study | N/A |
| pCCFP-BDR3 | This study | N/A |
| pCCFP-BDR2as | This study | N/A |
| pCCFP-BDR3t | This study | N/A |
| pTA7002 | 33 | N/A |
| pTA7002-BDR1-HA | This study | N/A |
| pTA7002-BDR2-HA | This study | N/A |
| Software and algorithms | | |
| STAR v2.5.2b | 34 | https://github.com/alexdobin/STAR |
| samtools 1.3.1 | 35 | http://www.htslib.org/ |
| featureCounts function from Rsubread package 1.24.2 | 36 | https://www.bioconductor.org/packages/3.4/bioc/html/Rsubread.html |
| Rsubread package 1.24.2 | 37 | https://www.bioconductor.org/packages/3.4/bioc/html/Rsubread.html |
| Bioconductor 3.4 | 38 | https://www.bioconductor.org/packages/3.4 |
| DEseq2 1.14.1 | 39 | https://www.bioconductor.org/packages/3.4/bioc/html/DESeq2.html |
| Trimmomatic 0.33 | 40 | http://www.usadellab.org/cms/?page=trimmomatic |
| Bowtie2 | 41 | N/A |
| Picard 2.2.4 MarkDuplicates | Broad Institute | http://broadinstitute.github.io/picard/ |
| rtracklayer | 42 | http://bowtie-bio.sourceforge.net/bowtie2/index.shtml |

(Continued on next page)

Continued

| REAGENT or RESOURCE | SOURCE | IDENTIFIER |
|------------------------------------|------------------|---|
| EnrichedHeatmap | ⁴³ | https://www.bioconductor.org/packages/3.4/bioc/html/EnrichedHeatmap.html |
| GeneNeighborhood package v 1.0 | Pascal GP Martin | https://github.com/pgpmartin/GeneNeighborhood |
| Scripts for ChIP-seq data analysis | Pascal GP Martin | https://github.com/pgpmartin/ChIPseq_functions |
| MxPro-Mx3000P v4.10 | Agilent | N/A |

RESOURCE AVAILABILITY

Lead contact

Further information and requests for resources and reagents should be directed to and will be fulfilled by the lead contact, Scott Michaels (michaels@indiana.edu).

Materials Availability

All unique/stable reagents generated in this study are available from the Lead Contact without restriction.

Data and code availability

The accession numbers for the transcriptome and ChIP-seq data reported in this paper are GEO: GSE112440, GSE112441, GSE113076, GSE113059, GSE113078, GSE131772.

This paper does not report original code.

Any additional information required to reanalyze the data reported in this paper is available from the lead contact upon request.

EXPERIMENTAL MODEL AND SUBJECT DETAILS

Arabidopsis thaliana was used in this study. All mutant and transgenic lines detailed in the [Key resources table](#) were in Col-0 background.

METHOD DETAILS

Plant growth conditions

fpa-7, *flk*, *ld-1*, *flc-3*, *brd1-1*, *brd2-1* and *brd3-1* have been described previously.^{13,31} Seeds were surface sterilized with 70% ethanol for 10 min, plated on ¼ Murashige and Skoog medium, and stratified for 3 days at 4°C, to promote germination. *Arabidopsis* plants were grown in temperature-controlled rooms at 22°C in long days (16-h light/8-h dark) under cool-white fluorescent light with a light intensity of approximately 125 μmol m⁻² s⁻¹. For vernalization treatment, imbibed seeds were cold treated for 30 days. Tobacco plants were grown in temperature-controlled rooms at 22°C in short days (8-h light/16-h dark) under cool-white fluorescent light with a light intensity of approximately 125 μmol m⁻² s⁻¹.

Constructs

cDNAs and genomic DNAs were amplified, cloned into pENTR/D-TOPO (Invitrogen), and confirmed by Sanger sequencing. For Y2H screening and pairwise interaction assays, cDNAs with stop codons were transferred to pDEST32 and pDES22 using LR Clonase (Invitrogen) according to the manufacturer's instructions. For BiFC, cDNAs with stop codons were then transferred to pNYFP-X-gw and pCCFP-X-gw by LR reaction. BDR1-MYC, BDR2-MYC, and BDR3-MYC have been described previously.¹³

Y2H

Full length FPA was used as a bait to screen a cDNA library prepared from vegetative shoot apices. Screening was performed by growing yeast on SC–Trp–Leu–His + 3AT (25 mM) plates and followed by X-gal assays. Pairwise interaction assays were carried out on SC-Trp-Leu-His +3AT or SC-Trp-Leu-Uracil plates.

BiFC

Proteins were fused with either the N-terminal portion of enhanced Yellow Fluorescent Protein (eYFP) or the C-terminal portion of enhanced Cyan Fluorescent Protein (eCFP) as described previously.³² Constructs were transformed into *Agrobacterium tumefaciens* strain C58C1³⁰ by electroporation. Agrobacteria with constructs were grown overnight (16 h) at 28°C and then resuspended at OD_{600nm} of 0.4 in 10 mM MgCl₂ and 100 μM acetosyringone (Sigma). The Agrobacteria suspensions were mixed in equal volume for transient transformation. Paired constructs were cotransformed into young leaves of 4-week-old tobacco plants. Infiltrated plants were grown for 48 h under 8 h light/16 h dark conditions, then imaged using a Leica SP5 confocal microscope.

Co-immunoprecipitation and mass spectrometry

Nuclei were isolated from 3-day-old seedlings as described previously.⁴⁴ Nuclei were resuspended in Extraction Buffer (50 mM Tris-HCl, pH 7.5, 150 mM NaCl, 5 mM MgCl₂, 10% glycerol, 0.1% NP-40, 1 mM PMSF, 2 mM DTT and 1:300 Plant Protease Inhibitors (Sigma)) and were passed through a 27G ½ needle six times after being frozen and thawed three times. The nuclear extracts were centrifuged twice at 13000 rpm for 15 min at 4°C and supernatants were transferred to new tubes. Immunoprecipitation was performed as described previously with minor modifications.⁴⁵ Briefly, the nuclear extracts were incubated with Agarose-protein A-bead-conjugated anti-FPA rabbit polyclonal antibodies, which were raised against C-terminal portion (536-901) of FPA protein (Covance), for 1 h on a rotating platform. The complexes were then washed for 5 min with Extraction Buffer (8 times in total), resuspended in SDS loading buffer, and then boiled for 5 min before being resolved on 10% SDS-PAGE gel. Gel strips were then subjected to LC-MS/MS.

For transient co-expression, FPA-MYC, BRD1-HA, BRD2-HA fusions were cloned into pTA7002³³ and transformed into *Agrobacterium tumefaciens* strain C58C1.³⁰ Paired constructs were co-transformed into young leaves of 4-week-old tobacco plants. Forty h after infiltration, leaves were sprayed with 50 μM dexamethasone and harvested after 6 h. Co-immunoprecipitation was performed as mentioned above. The immunocomplexes were resolved on 10% SDS-PAGE gel and transferred to nitrocellulose membrane for probing with anti-HA-peroxidase (Sigma) and then, after stripping the membrane, anti-c-Myc-peroxidase (Sigma). Signals were detected using SuperSignal West Pico Chemiluminescent Substrate (Thermo Scientific).

RNA expression analysis

Expression analysis was performed as described previously.¹³ Briefly, RNA was isolated from 8-day-old seedlings using the Spectrum Plant Total RNA kit (Sigma) and quantified with a NanoDrop 2000 Spectrophotometer. 3 μg of total RNA was reverse-transcribed into cDNA with SuperScript III reverse transcriptase (Invitrogen) and 500 ng of oligodT primer. The resulting cDNAs were diluted 10-fold. 20 μL quantitative PCR reactions were performed using 10 μL Platinum SYBR Green qPCR SuperMix-UDG kit (Invitrogen), 2 μL of diluted cDNA, 0.5 μL each primer (4 μM), 0.04 μL ROX reference dye, and 6.96 μL H₂O. qPCR reactions were performed on a Mx3005P Real-Time PCR System (Agilent) (50°C for 2 min, 95°C for 5 min, 50 cycles of 95°C, 5 s, 60°C, 20 s, 72°C, 10 s; 1 cycle of 95°C 1 min, 55°C 30 s, 95°C, 30 s). Relative and absolute quantification were determined against the standard curves using MxPro QPCR software (the standard curves were made by sequentially diluting the synthesized cDNA four-fold until 1/1024; a no reverse transcriptase control was included as a negative control). *ACTIN 2* was used as a reference gene. The integrity of the final qPCR products was determined by melting curve analysis. The relative amount of *FLC* mRNA was normalized to the level of *ACTIN 2*.⁴⁶ All experiments were repeated at least three times with similar results.

RNA-seq

As detailed in GEO: GSE112441, total RNA was extracted from three independent replicates of 8-day old seedlings from each genotype using Trizol reagent (Invitrogen) following the manufacturer's instructions. Libraries were prepared from 1.5 μg of total RNA using Illumina TruSeq Stranded mRNA Library Prep kit. Libraries were sequenced on a NextSeq500 instrument at Indiana University Center for Genomics and Bioinformatics.

ChIP-qPCR

ChIP was performed as described previously.³¹ Briefly, seeds were sown on Murashige and Skoog medium and stratified for 4 days at 4°C. Whole 7-day-old seedlings grown under long-day conditions were harvested and fixed with 1% formaldehyde. Cross-linked samples were homogenized in lysis buffer (50 mM HEPES pH 7.5, 150 mM NaCl, 1 mM EDTA, 1% Triton X-100, 0.1% sodium dodecyl sulfate, 0.1% SDS, 2 mM DPDS, 1 mM PMSF, and 1:300 Plant Protease Inhibitors (Sigma)) and sheared by sonication. The homogenates were centrifuged twice at 13000 rpm for 15 min at 4°C and the supernatants were transferred to new tubes. The supernatants were precleared with salmon sperm DNA/protein A agarose slurry. The precleared samples were incubated with the antibodies against anti-H3K4me3 (17-614, Millipore) or H3K27me3 (07-449, Millipore). The protein A agarose/antibody/histone complexed were washed twice with Low Salt Immune Complex Wash buffer, once with High Salt Immune Complex Wash buffer, once with LiCl Immune Complex Wash buffer, and twice with TE Buffer. Precipitated DNA samples associated with modified Histone H3 were relatively and absolutely quantified with real-time PCR, similar to the RNA expression analysis (above) except using sonicated genomic input DNA to generate standard curves. Histone H3K4me3 and H3K27me3 enrichments at *FLC* locus were normalized against the *ACTIN 2*⁴⁶ locus. Data presented are an average of three replicates. Primers shown in Table S3.

ChIP-seq

Nuclei were isolated from cross-linked samples described as previously⁴⁷ and were then resuspended in nuclei lysis buffer (50mM Tris-HCl pH8, 10mM EDTA, 1% SDS, 1mM PMSF, 1% Plant Protease Inhibitors (Sigma)). After fragmentation using a Covaris S200, the chromatin samples were diluted with ChIP dilution buffer (1.1% Triton X-100, 1.2mM EDTA, 16.7mM Tris-HCl pH8.0, 167mM NaCl, 1mM PMSF, 1% Plant Protease Inhibitors (Sigma)). Diluted chromatin samples were subjected to immunoprecipitation with antibodies (anti-FPA; anti-RNA polymerase II CTD repeat YSPTSPS antibody (8WG16), Abcam ab817; and control IgG Abcam ab18413) described as above.

Native histone ChIP was largely performed as described previously,⁴⁸ with anti-Histone H3 Abcam ab1791, anti-Histone H3 (tri methyl K36) Abcam ab9050, anti-Histone H3 (tri methyl K4) Millipore 17-614, and anti-Histone H3 (di methyl K4) Millipore 17-677.

ChIP libraries were prepared using NEBNext Ultra DNA Library Prep kit (New England Biolabs) and sequenced on the NextSeq 500 platform at Center of Genomics and Bioinformatics, Indiana University.

Reanalysis of published datasets

In the present work, we used some sequencing datasets that we or other groups have previously published and that are publicly available from Gene Expression Omnibus (<https://www.ncbi.nlm.nih.gov/geo/>). Our RNA-seq data in *bdr* mutants (GEO: GSE112441), but not in the *fpa* mutant (also in GEO: GSE112441) was previously reported in Yu et al.¹³ An independent RNA-seq experiment is also available for *fpa* mutant in GEO: GSE112440. Our ChIP-seq data for BDR1, BDR2 and BDR3 (GEO: GSE113059 and GEO: GSE131772) were first reported in Yu et al.¹³ and analyzed for gene sets distinct from those in the present article. Similarly, our Pol II ChIP-seq data (GEO: GSE113078) was previously analyzed¹³ on other gene sets. Our ChIP-seq data for FPA (GEO: GSE113059) was not reported previously but was re-analyzed in Parker et al.⁴⁹ with a specific pipeline, different from the one used here and described in GEO: GSE11359. DNase hypersensitivity (DHS) data is from Zhang et al.⁵⁰ and is available in GEO: GSE34318. DNase-seq reads from the 3 replicates of wild-type seedlings were retrieved, trimmed with Trimmomatic 0.33,⁴⁰ remapped to TAIR10 using bowtie⁵¹ allowing no mismatches (-v 0 -m 1-strata-best) and merged in a single bam file. The reads were shifted to be centered on their 5' ends before computing the coverage using R/bioconductor GenomicRanges functions.³⁸ GRO-seq and RNA-seq data from Hetzel et al.⁵ (GEO: GSE83108) were trimmed with Trimmomatic 0.33 and reads longer than 20bp were re-mapped on TAIR10 using STAR 2.5.2b.³⁴ Uniquely mapped reads with a mapping quality > 10 were selected using samtools 1.3.1³⁵ to compute the strand-specific coverages using GenomicRanges functions.

Bioinformatic analyses

Raw and processed ChIP-seq and RNA-seq data, along with detailed experimental and bioinformatic procedures are provided in GEO: GSE112443 and its subseries. TAIR10 annotations (<https://www.arabidopsis.org/>) were used for all analyses. Blacklisted regions for ChIP-seq experiments were described previously.¹³

RNA-seq computational analysis

RNA-seq data from GEO: GSE112440 were normalized as FPKM and used to define 9 groups of protein-coding genes differing by their average FPKM levels in 8 day-old Col-0 seedlings. The corresponding groups are provided as Table S1 in Yu et al.¹³ RNA-seq data from GEO: GSE112441 was used for differential expression analysis and all other analyses presented in this article. Paired-end reads (2x43bp) were mapped to TAIR10 genome using STAR v2.5.2b³⁴ with default parameters. Reads with mapping quality below 10 were removed using samtools 1.3.1³⁵ and those uniquely mapping to TAIR10 annotated genes were counted with featureCounts³⁶ from the Rsubread package 1.24.2³⁷ of R 3.3.2 and Bioconductor 3.4.³⁸ Analysis of differentially expressed protein-coding genes between wild-type Col-0 seedlings and single mutants for *bdr1*, *bdr2*, *bdr3*, *fpa* or *bdr1,2,3* triple mutant was done with DESeq2 1.14.1.³⁹ A table of differentially expressed genes and corresponding statistics (logFC, raw p value and adjusted p value for all comparisons) is provided as Table S2. We also defined a set of 1408 control, non-differentially expressed genes ("Not DE") by selecting genes with high p values ($p < 0.45$) and low absolute $\log_2(\text{fold-change}) < 0.25$ for all comparisons (single *bdr1*, *bdr2*, *bdr3* and *fpa* mutants and the *bdr1,2,3* triple mutant versus wild-type) and removing genes with extreme read counts (DESeq2 basemean > 3 and < 1e5), as previously described.¹³

ChIP-seq computational analysis

Adaptor sequences were removed from paired-end reads using Trimmomatic 0.33⁴⁰ and aligned to the *Arabidopsis* genome using Bowtie2.⁴¹ Duplicate fragments (Picard 2.2.4 MarkDuplicates) and low quality alignments (MapQ < 2, samtools 1.3) were removed. For MNase-seq and ChIP-seq for histone modifications, fragment sizes between 70bp and 250bp were kept for analysis. Aligned reads were imported in R (v.3.3.2) to obtain coverages using Bioconductor v3.4.⁵² Coverages were normalized as fragments per 10 million fragments (FP10M) and exported to bigWig files with the rtracklayer package.⁴² ChIP-seq peaks were detected using MACS2 2.1.0⁵³ in paired-end mode. Peaks located in blacklisted regions were removed. Average profiles and metagene plots were produced as described in Yu et al.¹³

Multigene heatmaps

Multigene heatmaps were produced with the EnrichedHeatmap package⁴³ from coverages (in FP10M) that were averaged in 20bp bins before/after genomic features of interest (TSS, TES or peak center) or in bins covering every 1% of gene length along gene bodies. Changes in histone modification and Pol II were evaluated by calculating the difference between the binned coverage in *bdr1,2,3* mutant and the binned coverage in wild type before producing the heatmaps.

QUANTIFICATION AND STATISTICAL ANALYSIS

For flowering time analysis (Figures 2A, 2B, and 2E) $n = 18$ plants for each genotype. RT-qPCR (Figures 2C and 2D) and ChIP-qPCR (Figure 2G) data was acquired using MxPro-Mx3000P v4.10 QPCR SOFTWARE. The statistical test used, the p value threshold, and the meaning of error bars are indicated in the legend of Figure 2. The significance of the intersection between genes regulated in *bdr1,2,3* and *fpa* (Figure 3B) was evaluated using Fisher exact test (fisher.test function in R 3.3.2) and the corresponding p value is indicated in Figure 3B. As indicated in the legend of Figure 4, the differences in the expression of genes from the different groups shown in Figures 4B and 4D were evaluated by Wilcoxon rank sum test (R 3.3.2).